Available online at www.sciencedirect.com
SCIENCE DIRECT®
Fluid Phase Equilibria 224 (2004) 221–230
FLUID PHASE EQUILIBRIA
www.elsevier.com/locate/fluid

A molecular dynamics study of a liquid–liquid interface: structure and dynamics

Jörn B. Buhn [a,*], Philippe A. Bopp [b], Manfred J. Hampe [a]

[a] *Fachgebiet für Thermische Verfahrenstechnik, Technische Universität Darmstadt, D-64287 Darmstadt, Germany*
[b] *Laboratoire de Physico-Chimie Moléculaire (LPCM), Université Bordeaux 1, F-33405 Talence Cedex, France*

Received 22 August 2003; received in revised form 16 February 2004; accepted 20 February 2004

Abstract

The liquid–liquid (L/L) interface between two partially miscible model Lennard–Jones fluids is investigated in the temperature range $100\,K \leq T \leq 138\,K$ using molecular dynamics computer simulations. The equilibrium compositions in the two phases agree reasonably well with recent results from DFT theory. The structure of the L/L interface is characterized in terms of partial density profiles of the two components and the interfacial tensions are computed for all temperatures using the virial method. The self-diffusion coefficients are determined as a function of temperature and distance from the interface and are compared to the ones of the pure liquids under identical conditions. A slight anisotropy is found in the interfacial system. It is restricted to the regions of strong variations of the partial density profiles and is due to an enhancement of the tangential components of the self-diffusion coefficients compared to the components $D_{s,N}$ normal to the interface.

Keywords: Molecular dynamics; Liquid–liquid equilibria; Lennard–Jones mixture; Interfacial structure; Diffusion coefficient

1. Introduction

A detailed understanding of liquid–liquid (L/L) interfaces between two partially miscible liquids is of great importance in such areas as chemical engineering, chemistry or biology. In particular, the ubiquitous mass transport phenomena through these interfaces, whether occurring in an extraction column or in a biological system, are poorly understood. This can be ascribed to the very nature of this interface, which makes experimental probing extremely difficult. Even though decisive improvements have been made in the fields of X-ray or neutron scattering investigations [1,2], a detailed microscopic description of the liquid interface, e.g. partial density profiles or molecular orientations at the interface, is still lacking. In a simple picture, the overall transport of a species through a fluid interface will be related to the particle mobilities near or at the interface and in the two phases on either side of the interface. However, it is not clear how these two phenomena could be clearly distinguished. It is, for instance, not even clear what the spatial dimension, say the width, of the "interface" could be and how far into the adjacent phases its influence on mass transfer might extend. In order to try to understand all this it is clear that much more insight into the structure and the dynamics in this entire region is needed.

One approach to study this problem is computer simulations: molecular dynamics (MD) simulations have been shown to be an efficient theoretical tool for studying L/L interfaces [3]. In the last decade MD investigations of structural and dynamical interfacial properties started with liquid–vapor systems of pure components [4–12] or binary mixtures [13–16]. These systems could be studied with the computational resources available at the time since they can be easily generated and equilibrated. Studies on L/L interfaces followed, concerning either simple Lennard–Jones-(LJ)-model fluids [16–18] or more complex molecular fluids [19–22]. However, little is known about the dynamical behavior of the particles in an interfacial system. Moreover, partially contradictory results have been reported [23–25] concerning the question whether, and how much, the normal or the tangential component of the self-diffusion coefficient changes at the interface. In the present work, we would like to contribute to resolving this question by

* Corresponding author.
E-mail addresses: buhn@tvt.tu-darmstadt.de (J.B. Buhn), pab@hulot.lsmc.u-bordeaux.fr (P.A. Bopp), hampe@tvt.tu-darmstadt.de (M.J. Hampe).

0378-3812/$ – see front matter © 2004 Elsevier B.V. All rights reserved.
doi:10.1016/j.fluid.2004.02.012

investigating the structural as well as the dynamical character of an L/L interfacial system focusing on the partial density profiles, the resulting interfacial thicknesses and the self-diffusion of particles in this region.

The paper is structured as follows. First, the modeling and simulation details will be discussed in Section 2. Here the emphasis is put on demonstrating that we start our production runs from properly equilibrated systems, i.e. without having to expect any global composition changes during the production runs. We will proceed to discuss the compositions of the two phases and describe the structure of their interface by means of the partial density profiles in Section 3.1. In Section 3.2, we will deal with the variation of the self-diffusion coefficients in the L/L interfacial systems. We will focus in particular on the differences between self-diffusion in the bulk phases and near the interface, i.e. where the system becomes anisotropic. Conclusions will finally be drawn in Section 4 with some outlook for future work.

2. Model and computations

2.1. Interaction potential and mixing rules

We consider simple model fluids consisting of two different Lennard–Jones (LJ) species, labeled here for simplicity Ar1 and Ar2. It is known [26,27] that the classical LJ interaction potential:

$$\phi(r) = 4\epsilon \cdot \left[\left(\frac{\sigma}{r}\right)^{12} - \left(\frac{\sigma}{r}\right)^{6}\right] \quad (1)$$

together with the Lorentz–Berthelot (LB) mixing rules does not lead to stable L/L systems. This is because according to this rule the interaction parameter $\epsilon_{\mathrm{Ar1–Ar2}}$ between the unlike species is intermediate between the two ϵ-values for like–like interaction, i.e. this potential well is deeper than the one of the weakest interaction between like particles (here chosen to be $\epsilon_{\mathrm{Ar1–Ar1}}$). Thus, in order to obtain a stable (or at least metastable [26]) L/L interfacial system a new parameter ξ is introduced into the Berthelot rule which decreases the depth of the potential well between unlike particles, i.e.:

$$\epsilon_{\mathrm{Ar1–Ar2}} = \xi(\epsilon_{\mathrm{Ar1–Ar1}}\epsilon_{\mathrm{Ar2–Ar2}})^{1/2}, \quad (2)$$

Table 1
Like and unlike Lennard–Jones interaction parameters

	ϵ/k (K)	σ (Å)
Ar1–Ar1	155	3.504
Ar1–Ar2	133.6	3.504
Ar2–Ar2	180	3.504

$$\sigma_{\mathrm{Ar1–Ar2}} = \tfrac{1}{2}(\sigma_{\mathrm{Ar1–Ar1}} + \sigma_{\mathrm{Ar2–Ar2}}). \quad (3)$$

In comparison with previous work [17,18] where zero attraction between unlike particles causes total immiscibility we allow here for a realistic miscibility by choosing a factor of $\xi = 0.8$. Depending on the diameter ratio σ_{11}/σ_{22} and on the well-depth ratio $\epsilon_{11}/\epsilon_{22}$ immiscibility is expected to occur for $\xi \leq 0.8$ [27,28]. A complete list of the LJ parameters used in this work is found in Table 1. Note, in particular, that the σ-parameters are identical for both species, and so are their masses, 39.95 a.u. (Argon). This setup does not correspond to any 'real' chemical system. It was chosen here as the starting point for systematic studies of the influence of the potential parameters and masses on the structural and dynamic properties of these systems.

2.2. System setup and equilibration

We investigate six different L/L systems with varying compositions of the bulk phases at six temperatures ranging from $T = 100$ to 138 K and at ambient pressure. Due to its three-dimensional periodicity the simulation box contains two L/L interfaces, infinitely extended in the x- and y-directions, separating an Ar2-rich phase from an Ar1-rich one, see Fig. 1, where the Ar1-rich phase appears inside between the two halves of the Ar2-rich one in the periodic system. Equilibration was started from a lattice structure of a total of $N = 6144$ particles already arranged according to the appropriate liquid equilibrium composition. The data for these phase equilibria were obtained from density functional theory (DFT) calculations, where a mean-field approximation concerning the attractive interaction is applied, with a code supplied by Winkelmann [29]. This procedure is computationally fast (seconds on a PC), similarly an equation of state approach [30,31] could have been used. In the same way the critical temperature at which the system reaches

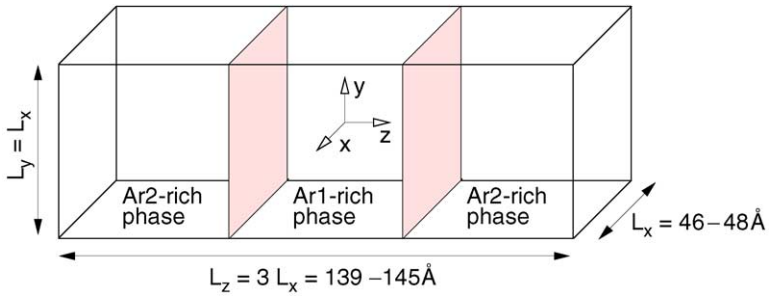

Fig. 1. Schematic representation of the simulation box with the two outer Ar2-phases and the Ar1-phase in the middle.

Table 2
Phase equilibria data from DFT-calculations [29] used as starting values for the MD simulations in this work. The mole fractions of the minority components and the total bulk densities ρ_{Ar2}-rich phase, ρ_{Ar1}-rich phase are given for both bulk phases

T (K)	x_{Ar1} Ar2-rich phase (–)	x_{Ar2} Ar1-rich phase (–)	ρ_{Ar2}-rich phase (Å^{-3})	ρ_{Ar1}-rich phase (Å^{-3})
100	0.0128	0.0163	0.0194	0.0184
108	0.0208	0.0267	0.0188	0.0178
116	0.0322	0.0418	0.0183	0.0171
126	0.0532	0.0707	0.0176	0.0163
132	0.0709	0.0961	0.0171	0.0157
138	0.0944	0.1313	0.0166	0.0152

complete miscibility was estimated to be $T_c = 158$ K. In Table 2, the mole fractions x_{Ar1} in the Ar2-rich phase and x_{Ar2} in the Ar1-rich phase resulting from these calculations are given together with the total number density $\rho_{Ar1\text{-rich phase}}$ and $\rho_{Ar2\text{-rich phase}}$ of both liquid bulk phases.

Starting thus with reliable values for the compositions of the inhomogeneous L/L systems, constant compositions in the two bulk phases could be expected after only relatively short equilibration runs. These equilibrations were performed in the NpT-ensemble over a period of 1.5 ns (300,000 integration steps with a timestep of $\Delta t = 0.005$ ps) using the Berendsen thermo- and barostat [32] with relaxation times of $\tau_T = 0.5$ ps and $\tau_p = 2.0$ ps, respectively. The partial density profiles were determined from subsequent production runs of 1.5 ns in the same ensemble. Thereafter, second production runs of 50 ps (10,000 steps) were carried out yielding 5000 configurations which were later used to compute the velocity autocorrelation functions (VACF) and the mean square displacements (MSD) to obtain self-diffusion coefficients.

To ensure that truly stable phase equilibria had been reached we extended the length of the production for the lowest temperature case, $T = 100$ K, where slow equilibration could be expected, up to 7.5 ns (1.5×10^6 steps). No significant drift or change of the partial density profiles could be detected. In another test a simulation was started with the compositions of the two bulk phases deliberately out of equilibrium. This was done by instantaneously heating up the $T = 100$ K-L/L system to $T = 138$ K in an NpT-simulation. In this way, we could examine the evolving composition changes as well as the variation of the partial density profiles. The result is shown in Fig. 2 where the continuous lines represent the initial system at $T = 100$ K (out of equilibrium) and the target state at $T = 138$ K. The dotted lines between depict the profiles after 1.25 ns and after subsequent time increments up to 10 ns. The first profiles after 1.25 ns are already quite different from the initial $T = 100$ K-profiles. This jump in the profile shapes results essentially from the relatively rapid volume expansion in the NpT-simulation due to the increased temperature. Thereafter slower modifications of the profiles are observed since henceforth only mass transfer of either component

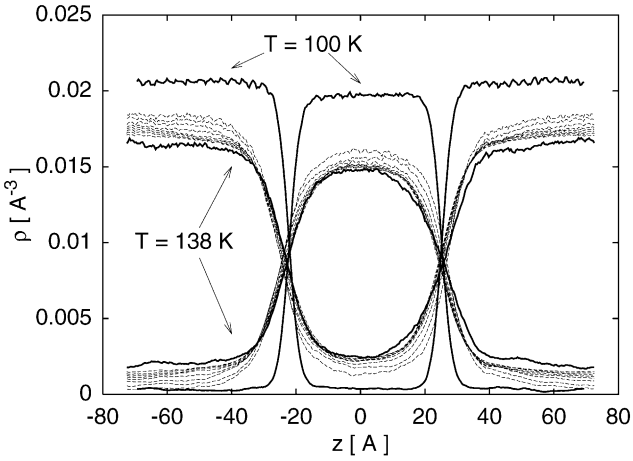

Fig. 2. The initial L/L system at $T = 100$ K is instantaneously heated up to $T = 138$ K. The continuous lines represent the partial density profiles of the initial and target state, respectively. The dotted lines which depict the partial density profiles after 1.25, 2.25, 3.75, 5, 6.25, 7.5, 8.75 and 10 ns are gradually approaching the target profile at $T = 138$ K.

determines the process. The most persisting features are the small oscillatory structures seen in the partial density profiles of the majority components at $T = 100$ K, see Fig. 2. They could be smoothed progressively only in the most extended production run, see Section 3.1.2.

The parallel version of the DL_POLY [33] program package was used on a Linux-cluster for all simulations. For the integration a multiple timestep Verlet algorithm with a primary cut-off radius of $r_{cut,prim} = 14.4$ Å and a secondary cut-off of $r_{cut,sec} = 18.0$ Å was applied. Interactions with particles located between $r_{cut,prim}$ and $r_{cut,sec}$ were calculated every 10th timestep. A large cut-off value, larger than the width of the interface, is certainly needed to catch the influences of the two phases on the interface. On the other hand, the two interfaces should be independent, i.e. the box length $\langle L_x \rangle$ (see Fig. 1) should not fall below 12σ and $\langle L_z \rangle$ should be at least $3\langle L_x \rangle$ [34,35]. It turned out from a test simulation with a maximum cut-off of half the smallest box dimension, $\langle L_x \rangle = 48.5$ Å, that no differences in the partial density profiles or the structure of the interface could be found compared with the ones obtained with the standard cut-off values given above. This test was done for the high temperature case, $T = 138$ K, where the interfacial domain is largest and the influence of the cut-off radius was expected to be crucial.

3. Results

3.1. Structural properties

3.1.1. Phase equilibria

The phase equilibria data resulting from the MD simulations, i.e. the mole fractions of the minority components and the partial densities ρ_{Ar1} and ρ_{Ar2} in both regions away

Table 3
Phase equilibria data from this work. Mole fractions of the minority components and partial densities ρ_{Ar1}, ρ_{Ar2} for the Ar1-rich as well as for the Ar2-rich phase

T (K)	x_{Ar1} Ar2-rich phase (–)	x_{Ar2} Ar1-rich phase (–)	ρ_{Ar1} Ar2-rich phase (Å^{-3})	ρ_{Ar2} Ar2-rich phase (Å^{-3})	ρ_{Ar1} Ar1-rich phase (Å^{-3})	ρ_{Ar2} Ar1-rich phase (Å^{-3})
100	0.015	0.013	0.000313	0.0206	0.0198	0.000256
108	0.022	0.027	0.000441	0.0200	0.0190	0.000525
116	0.035	0.041	0.000695	0.0193	0.0183	0.000786
126	0.062	0.070	0.001199	0.0182	0.0170	0.00129
132	0.086	0.099	0.001626	0.0173	0.0160	0.00177
138	0.108	0.142	0.001995	0.0165	0.0148	0.00244

from the interface, see below, are given in Table 3. Numerical values for the partial and total densities as well as for the compositions of the phases were obtained by fitting a function $\rho(z)$ [36,37]:

$$\rho(z) = \frac{1}{2}(\rho_1 + \rho_2) - \frac{1}{2}(\rho_1 - \rho_2)\tanh\left(\frac{2(z - z_i)}{w}\right) \quad (4)$$

to the simulated partial density profiles shown in Fig. 4. Therein, z is the direction normal to the interface, ρ_1 and ρ_2 are the partial densities of the coexisting bulk phases, z_i denotes the position of the interface (or more precisely the position of Gibbs' dividing surface) and w is a measure of the width of the interface. We estimate the uncertainties in the densities of the major components to be less than about 4% and those of the mole fractions to be of the order of $\Delta x = 0.0045$. Compared to the values from the DFT-calculations, Table 2, used to generate the initial configurations of the simulations, the simulated mole fractions x_{Ar1} in the Ar2-rich phases are slightly higher while the ones for Ar2 in the Ar1-rich phase agree completely within the uncertainties, except for the highest temperature. Fig. 3 shows both sets of data. The asymmetry in solubility, i.e. the

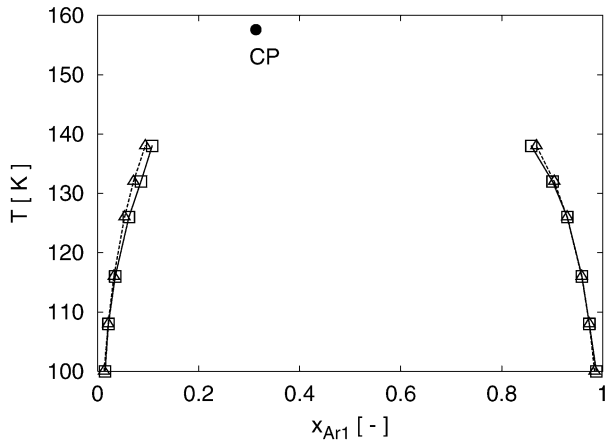

Fig. 3. T–x_{Ar1} diagram obtained for the bulk regions away from the interface from this work (□) and from DFT-calculations [29] (△). The critical point (CP) is estimated by Ref. [29] to be at $T_c = 158$ K and $x_{Ar1} \approx 0.32$.

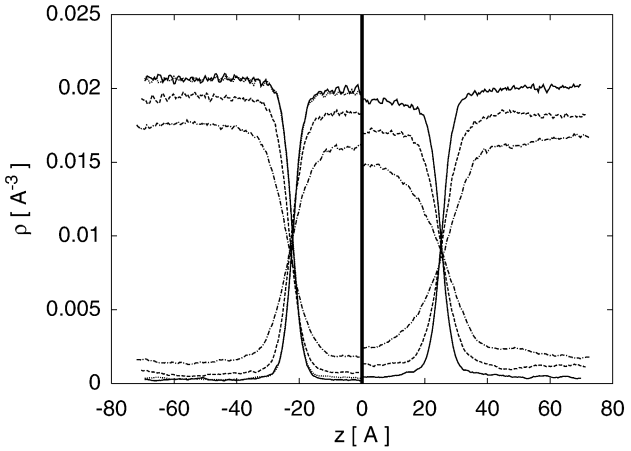

Fig. 4. Partial number density profiles ρ_{Ar1} and ρ_{Ar2} for six different temperatures. (Left) $T = 100$ K (—), $T = 116$ K (- - -), $T = 132$ K (—·—), additional: $T = 100$ K for an extended production run of 7.5 ns (1.5×10^6 steps) (···). (Right) $T = 108$ K (—), $T = 126$ K (- - -), $T = 138$ K (—·—).

higher solubility of Ar2 in Ar1 compared to the one of Ar1 in Ar2, is thus similar, but somewhat reduced compared to the mean-field approach. The total densities from the MD simulations are generally about 10% higher than the corresponding DFT-results.

3.1.2. Partial density profiles and interfacial structure

Averaging over 1.5 ns of production one obtains symmetric number density profiles similar to the ones shown in Fig. 2. One half of these profiles (not symmetrized) is shown in Fig. 4 for all temperatures studied; for better legibility the partial density profiles ρ_{Ar1} and ρ_{Ar2} for $T = 100$, 116 and 132 K were drawn on the left-hand side of the figure whereas the $T = 108$, 126 and 138 K profiles are depicted on the right-hand side. An additional simulation was performed with a central Ar1-rich phase extended by 21 Å for the highest temperature to ensure that no artefact arises from the narrowing of the constant density part of the central Ar1-rich phase. No significant changes were found, we thus do not report these data separately.

For the calculation of the partial density profiles the box length L_z (see Fig. 1) was divided into 360 slabs with slab thicknesses of the order of $\Delta z \approx 0.4$ Å and data were collected every timestep during the production period. The high ρ_{Ar2} plateau values in the Ar2-rich phase decrease smoothly toward the Ar1-rich phase, and vice versa for the ρ_{Ar1}-values. Due to varying system volumes in the NpT-simulations the profiles show slightly different lengths, the box length increasing from $\langle L_z \rangle = 138.7$ Å at $T = 100$ K to $\langle L_z \rangle = 145.0$ Å at $T = 138$ K. The incidence of these variations on the shape of the interfacial structure was explored in systematic test simulations in the NVT-ensemble. No significant differences appeared in the shapes and widths of the profiles.

A measure for the interfacial width w is provided by Eq. (4) where the tanh -term is related to the van der Waals

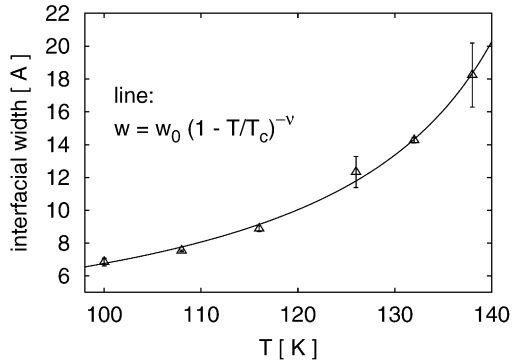

Fig. 5. Interfacial tension γ vs. temperature T. The results fit to the expression $\gamma = \gamma_0(1 - T/T_c)^{\mu}$ with $T_c = 158\,\mathrm{K}$, $\gamma_0 = 36.56\,\mathrm{mN/m}$ and $\mu = 1.32$.

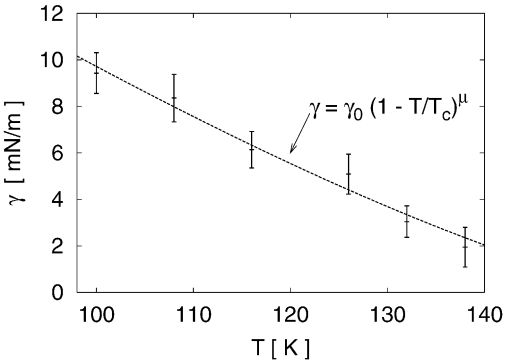

Fig. 6. Interfacial widths based on the tanh-profile in Eq. (4). The fitted line results from $w = w_0(1 - T/T_c)^{-\nu}$ with $w_0 = 2.66\,\text{Å}$, $T_c = 158\,\mathrm{K}$ and $\nu = 0.93$.

theory [38,39]. Averaging over both interfaces we obtained the results shown in Fig. 5; the error bars were estimated using the widths of the left and right interfaces. In addition, the function $w(T) = w_0(1 - T/T_c)^{-\nu}$ was fit to the width data, resulting in the continuous line in Fig. 5. The width increases from 6.9 to 18.2 Å (about 2σ–5.2σ) with increasing temperature, suggesting an expanded interfacial domain of several molecular diameters.

As mentioned above, the $T = 100\,\mathrm{K}$-system shows partial density oscillations in the ρ_{Ar1}- and ρ_{Ar2}-profiles after the normal production run of 1.5 ns (cf. e.g. [17,18,40]). These oscillations, which have a typical periodicity of about σ, can be ascribed to layering effects in the liquid. On one hand, this state point is close to the triple point, which makes melting of the lattice structure difficult; on the other hand, it could simply be still insufficient equilibration. Thus, in an extensive test simulation up to 7.5 ns (1.5×10^6 steps) we tried to separate these two effects. It turned out that the oscillatory structure of the profiles could be smoothed, but not totally eliminated at $T = 100\,\mathrm{K}$ (see $T = 100\,\mathrm{K}$-profiles in Fig. 2). This is in particular true for the Ar2-rich phase where the attractive interactions are stronger than in the Ar1-rich one. It is known that a proper liquid–solid phase transition, i.e. a crystal nucleation, is difficult to carry out in a MD simulation [41,42]. First-order phase transitions exhibit observable hysteresis which shifts the phase change well beyond the coexistence point. Thermodynamically a large free energy barrier, which is in the simplest case represented by the interfacial tension, separates the two phases. Hence, the simulation often results in a supercooled or a glassy state rather than in a solid crystal. We could exclude amorphous glass formation by checking the self-diffusion coefficients D_s (see below), which are small, but nevertheless of an order of magnitude appropriate to liquids ($D_s = 0.85 \times 10^{-9}\,\mathrm{m^2/s}$ for Ar2 in the Ar2-rich phase and $D_s = 1.57 \times 10^{-9}\,\mathrm{m^2/s}$ for Ar1 in the Ar1-rich phase). The test run also confirmed that the plateau values of the bulk densities as well as their slopes toward the interface remain stable (cf. Fig. 4).

3.1.3. Interfacial tension

The interfacial tension γ is closely related to the partial density profile: sharp profiles are associated with high interfacial tensions. The value of γ tends toward zero when approaching the critical point, where the interfacial domain diverges. The interfacial tension γ was calculated via the virial method using the expression [3]:

$$\gamma = \frac{1}{2A}\langle 2VP_{zz} - VP_{xx} - VP_{yy}\rangle, \tag{5}$$

where A is the total cross-sectional area of the interface, V is the (constant) system volume and $P_{\alpha\alpha}$ ($\alpha = x, y, z$ in the laboratory system) is a diagonal element of the pressure tensor. It can be expressed as

$$VP_{\alpha\beta} = \sum_i m_i \dot{r}_{i\alpha}\dot{r}_{i\beta} + \sum_{i<j} r_{ij\alpha} f_{ij\beta} \quad (\alpha, \beta = x, y, z), \tag{6}$$

where m_i is the mass of particle i, $\dot{r}_{i\alpha}$ is the component of its velocity in α-direction, $r_{ij\alpha}$ is the component of the intermolecular separation in α-direction and $f_{ij\beta}$ is the corresponding component of the force in β-direction. The first term in Eq. (6) accounts for the kinetic (ideal gas) contribution whereas the second one is due to the intermolecular interactions. Note that the area A in Eq. (5) denotes the whole interfacial area in the system, i.e. one has to take $A = 2L_xL_y$. Results were produced in two independent NVT-simulations of the equilibrated L/L system. We took the weighted averages of a 500 ps-run yielding 50,000 configurations and a 1500 ps-run yielding 15,000 configurations. The results for different temperatures are shown in Fig. 6. Error estimations were done using the blocking method of Flyvberg and Petersen [43].

As already mentioned, at the critical point the coexistence disappears and the two phases become one. In the same way, the interfacial tension has to vanish so that the temperature dependence of the interfacial tension is well described by the law resulting from the van der Waals theory [38]:

$$\gamma(T) = \gamma_0\left(1 - \frac{T}{T_c}\right)^{\mu}. \tag{7}$$

Using the value of $T_c = 158\,K$ from the DFT-calculations [29], we adjusted the values of the two constants γ_0 and μ to our data, yielding $\gamma_0 = 36.56\,mN/m$ and $\mu = 1.32$. The resulting curve is also shown in Fig. 6. The critical exponent μ is believed to be $\mu \approx 1.26$ [38]. Considering the size of our system, the agreement of the critical exponents μ within about 5% can be considered satisfactory.

3.2. Dynamic properties

In this section, we focus on the variation of the self-diffusion appearing in the L/L system. We will therefore determine the self-diffusion coefficients D_s of both species, Ar1 and Ar2, in the bulk phases as well as close to the interfaces for all six temperatures. The self-diffusion coefficient can be taken as a measure for the mobility of a single particle. To distinguish bulk regions from near-interface regions the simulation box was divided into seven slabs (1–7) of different sizes as is shown in Fig. 7. Since the interfacial positions z_i do not change significantly with temperature (<1.5 Å) it was possible to position two slabs (each 10 Å thick) left and right of both interfaces, keeping their positions fixed for all temperatures. Hence we denote slabs 2, 3 and 5, 6 as "interface slabs" whereas slabs 1, 4 and 7 represent the bulk phases. Other arrangements of the slabs, e.g. with the same width for all slabs throughout the simulation box, have also been tested. The present arrangement was found to be the most satisfactory one in terms of resolution and statistics. The width of the "interface slabs" was chosen so that a slab would contain half the density gradient at the highest temperature, $T = 138\,K$.

In equilibrium MD simulations the self-diffusion coefficients D_s can be calculated using either the Einstein relation or the Green–Kubo (GK) method. Evaluating the Einstein relation requires the boxshift-corrected particle positions $\vec{r}_i(t)$ to evaluate the mean-square displacements. Averaging over equivalent particles, one has

$$D_s = \lim_{t\to\infty} \frac{\mathrm{MSD}(t)}{t} = \lim_{t\to\infty} \frac{1}{6Nt} \left\langle \sum_{i=1}^{N} (\vec{r}_i(t) - \vec{r}_i(0))^2 \right\rangle. \quad (8)$$

In a similar fashion [44], on obtains D_s from the single particle velocity autocorrelation function $C_{vv}(t)$:

$$D_s = \frac{1}{3N} \int_0^\infty C_{vv}(t)\,\mathrm{d}t = \frac{1}{3N} \int_0^\infty \sum_{i=1}^{N} \langle \vec{v}_i(t) \cdot \vec{v}_i(0) \rangle\,\mathrm{d}t. \quad (9)$$

We applied Eqs. (8) and (9) separately to both components of the binary system in each of the seven slabs, binning the single particle functions according to the slab in which the particle is located at the time origin of the function. We thus obtain D_s-values associated with each species in each of the slabs.

This procedure agrees with that described by Davis [45], who defines a tracer diffusion coefficient in an inhomogeneous system as the one computed for tracer particles with an identical initial placement. To check the validity of this approach, the velocity autocorrelation functions $C_{vv}(t)$ were extended over $t_{corr} = 2.39$, 3.59, and 5.39 ps in order to detect a possible dependence of the results on the correlation length. A sensitivity of the results on the correlation length would indicate that the fixed allocation of a given particle to a given slab is no longer justified. However, we obtained, within error bars, identical values for the self-diffusion coefficients in all three cases.

In a second check, we have roughly estimated how many particles leave their initial slab within the correlation time. The distance covered by a particle in diffusive motion is estimated by the equation $\langle z \rangle = 2\sqrt{D_{s,z} t/\pi}$ [46], where $D_{s,z}$ denotes the self-diffusion coefficient in z-direction. In the most unfavorable case $D_{s,z} = 2 \times 10^{-9}\,m^2/s$ and the correlation length is 5.39 ps, leading to an average covered distance of less than 1.2 Å normal to the interface. This distance is small compared to the dimensions of the slabs and could be interpreted as some fuzziness of the slab boundaries. This agrees with the assumption of nearly unchanged compositions of the slabs during correlation.

Of course the statistical weights of the various VACFs will not be identical. It will be difficult to determine the self-diffusion coefficients of the minority components (Ar1

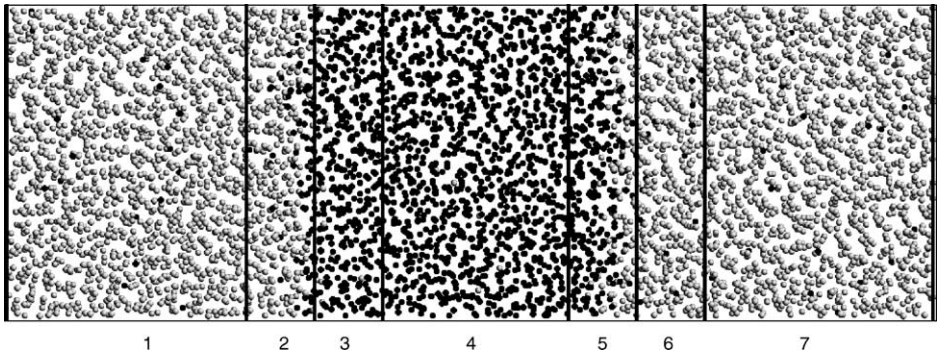

Fig. 7. Partitioning of the simulation box into seven slabs (1–7). The slabs 2, 3 and 5, 6 which have a width of 10 Å are positioned left and right of both interfaces. Slabs 1, 4, and 7 represent the bulk phases. Each slab contains both species Ar1 and Ar2. The picture shows a snapshot of the equilibrated $T = 100\,K$-system.

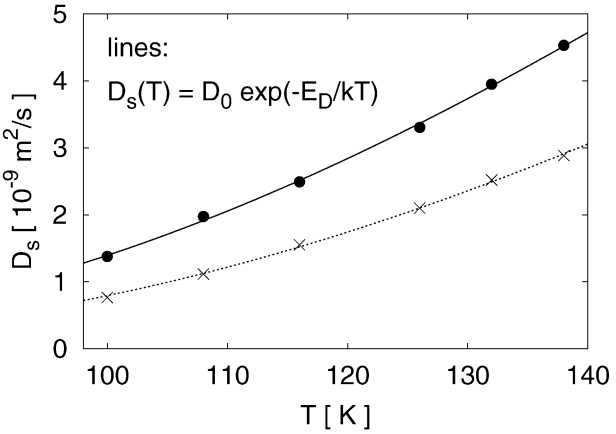

Fig. 8. Temperature dependence of the self-diffusion coefficient D_s for the pure species Ar1 (●) and Ar2 (×) from Eq. (9). The error bars are estimated to be about the size of the symbols. The lines represent the fitted Arrhenius function $D_s(T) = D_0 \exp(-E_D/kT)$ with the parameters reported in the text.

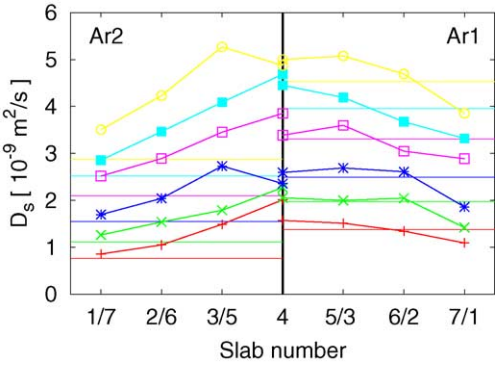

Fig. 9. Self-diffusion coefficients D_s of Ar1 and Ar2 in slabs 1–7 from Eq. (9). The central vertical line is a symmetry line. (Left) Self-diffusion coefficients D_s for Ar2. (Right) Self-diffusion coefficients D_s for Ar1. The highest lines represent the highest temperature $T = 138\,K$ whereas the lowest ones represent the lowest temperature $T = 100\,K$. The corresponding horizontal lines represent D_s for the pure components Ar1 and Ar2.

in the Ar2-rich phase, etc.), mainly at low temperatures. Furthermore, since the underlying data were produced in NpT-simulations, i.e. where the velocities are also manipulated by the thermostat, test NVE-simulations were made to ensure that the results are not influenced by this. Both ensembles provide similar self-diffusion coefficients within the expected statistical uncertainties. In another test the number of time origins over which Eqs. (8) and (9) are averaged was increased up to almost 5000; no significant difference to the results reported below could be detected.

As a reference we also determined the self-diffusion coefficients of pure Ar1 and pure Ar2 at the corresponding temperatures via both methods. Since the results agree, we show here only the GK-results in Fig. 8 along with plots of Arrhenius-fits of the form:

$$D_s(T) = D_0 \exp\left(-\frac{E_D}{kT}\right), \tag{10}$$

where D_0 is a pre-exponential factor and E_D is the so-called activation energy. We obtain values of 426.7 and 472.0 K for E_D/k, and 99.5×10^{-9} and $89.1 \times 10^{-9}\,m^2/s$ for D_0 for Ar1 and Ar2, respectively. As expected, due to the higher attractive forces among Ar2-particles, the mobility of these particles is smaller and the activation energy is higher. Depending on temperature the mobility of Ar1 is 1.6–1.8 times higher than that of Ar2.

3.2.1. Effects of composition on self-diffusion

First we want to investigate the effect of composition on self-diffusion. We consider therefore the bulk slabs 1, 4 and 7. In Fig. 9 the self-diffusion coefficients of Ar2 are shown on the left-hand side and those of Ar1 on the right-hand side, together with the ones for the pure phases (cf. Fig. 8). Where appropriate, the values were averaged over both corresponding slabs. It is found that the self-diffusion of Ar2 in the Ar2-rich phase (slab 1/7) as well as that of Ar1 in the Ar1-rich phase (slab 4) are both higher than in the corresponding pure systems. These deviations from the values in the pure liquids increase with increasing temperature (i.e. miscibility). The opposite is seen for Ar1 in the Ar2-rich phase (slabs 7/1): Here, the mobility of the solute particle is lowered compared to its behavior in the pure phase, in contrast to the self-diffusion of Ar2 in the Ar1-rich phase (slab 4), which is strongly increased. We note, however, that due to the small number of particles in these regions, the values for Ar2 in slab 4 and those for Ar1 in slabs 7/1 are statistically less reliable; there are e.g. only ≈26 Ar1-particles at $T = 100\,K$ in slab 7.

Two general trends can thus be extracted from these observations: (A) The self-diffusion is increased in the mixtures compared to the pure liquids. This could be ascribed to some sort of increased structural disorder, even though the σ-parameters of both species are identical. (B) The minority component tends to adopt the diffusive behavior of the majority component (i.e. Ar1 diffuses more slowly in Ar2 and Ar2 diffuses more rapidly in Ar1). The activation energies (divided by k) for both species are close to 490.0 K in the Ar2-rich phase and between 400 and 420 K in the Ar1-rich phase, thus close to the ones of the pure components.

3.2.2. Influence of the interface on self-diffusion

The self-diffusion near L/L interfaces, in particular the question whether it exhibits an anisotropy, has been studied by Meyer et al. [24] (see also [23]) and by Benjamin [25]. In both approaches the self-diffusion coefficient is split into a part tangential to the interfacial plane, $D_{s,T} = 1/2(D_{s,x} + D_{s,y})$, and another part normal to the interface, $D_{s,N} = D_{s,z}$. They both agree that $D_{s,T} > D_{s,N}$ at the interface, however, the arguments given differ. In the work of Meyer et al. [24], where an L/L interface between LJ-particles was investigated, $D_{s,T}$ and $D_{s,N}$ are similar in the bulk phase, as they should, and $D_{s,T}$ increases when approaching the interface.

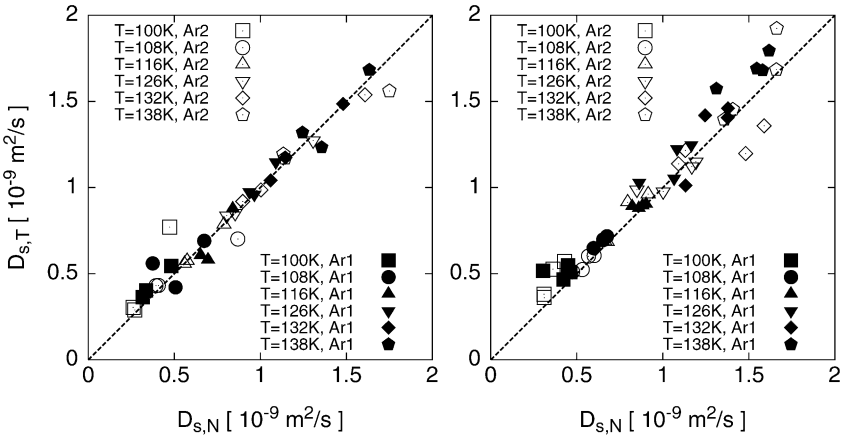

Fig. 10. The tangential component of the self-diffusion coefficient $D_{s,T}$ vs. the normal component $D_{s,N}$. (Left) Data for Ar2 (open symbols) and Ar1 (full symbols) in the bulk slabs 1, 4, and 7. (Right) Data for Ar2 (open symbols) and Ar1 (full symbols) in the interface slabs 2, 3, 5, and 6.

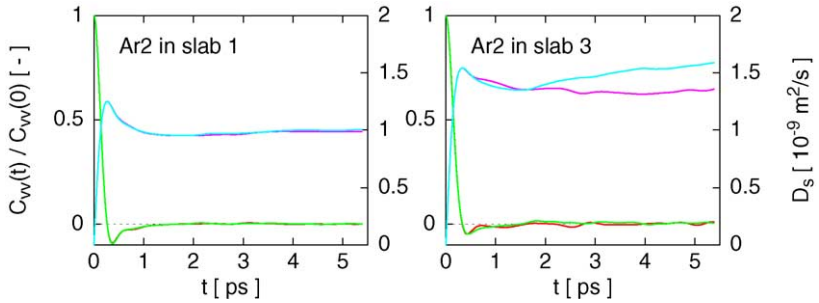

Fig. 11. Normalized VACF $C_{vv}(t)/C_{vv}(0)$ (left axes) and self-diffusion coefficients $D_s(t)$ (right axes) of Ar2 at $T = 132$ K. Tangential components: pale lines; normal components: dark lines; (left panel) in the bulk slab 1; (right panel) in the interface slab 3.

It is argued that the enhanced tangential mobility of the particles results from a decreased tangential pressure component P_T near the interface. On the other hand, Benjamin [25] investigated the L/L interface of water/1,2-dichlorothane and reports that $D_{s,T}$ remains almost constant throughout the system but that $D_{s,N}$ decreases in the vicinity of the interface for both liquids. This behavior was explained on the basis of a more structured water/1,2-dichlorothane interface and with restricted orientational dynamics at the interface. A third work [20] reports results from a water/2-heptanone system where anisotropic self-diffusion coefficients were found throughout the system for both species. However, the anisotropy is enhanced near the interface. It is concluded that the interface exerts a long range effect on the bulk phases which cannot be avoided in MD simulations due to immanent small box sizes.

In order to study these phenomena, the self-diffusion coefficients computed in the seven slabs were split into two parts, $D_{s,T}$ and $D_{s,N}$, as described above. Again the GK-results using Eq. (9) agreed well with the results of the Einstein method, Eq. (8). In Fig. 10, we have plotted the tangential part of the self-diffusion coefficient $D_{s,T}$ against the normal part $D_{s,N}$. The results from the "bulk slabs" (1, 4, and 7) are shown in the left plot and those from the "interface slabs" (2, 3, 5, and 6) appear in the right plot. As seen in the left panel of this figure, no anisotropy of D_s was found in the bulk slabs: the data are well grouped around the diagonal. The plot on the right-hand side, on the other hand, reveals a systematic slight anisotropy in favor of the tangential component $D_{s,T}$. In this, it agrees with the conclusions of Refs. [23,24]. On closer inspection, it seems that this anisotropy is enhanced with increasing temperature. To demonstrate the anisotropic behavior in terms of the VACF and its integral, Fig. 11 shows both curves (i.e. the perpendicular and parallel components) for Ar2 in the bulk slab 1 (left plot) as well as in the slab 3 near the interface (right plot) at $T = 132$ K. It is seen that in the bulk all curves coincide perfectly. In the interfacial region the VACF shows a smaller negative region (recoil), leading, as mentioned above, to a higher diffusivity. The anisotropy in D_s begins to appear after about 1.5 ps, a time much longer than the recoil time of about 0.5 ps. This indicates that it probably originates in many-body effects.

4. Summary, conclusions and outlook

We have examined the structural and dynamical behavior of L/L interfacial systems consisting of binary LJ-mixtures by means of MD simulations. This was done for six different temperatures ranging from $T = 100$ K, very close to the

triple point, to $T = 138\,\mathrm{K}$, which is approximately 20 K below the critical point. We show that the interfacial particle density profiles have widths of several molecular diameters and that these widths increase with increasing temperature.

The dynamics was investigated in terms of the self-diffusion. It is found to be composition dependent with the general trends that it is enhanced in mixtures compared to pure phases and that the minority species tends to diffuse like the majority one. We note here again that our particles have identical masses and sizes (LJ σ-parameters) and differ only in the depths of their interaction potentials. In keeping with previous work on similar systems, a slight anisotropy of the diffusion is found in the interfacial region, i.e. where the partial densities are not constant. There, the tangential mobility is slightly enhanced compared to the normal one. This was found for both species and at all temperatures. No anisotropy could be detected beyond this region.

This first investigation certainly opens up a set of new questions. It would thus be interesting to investigate mixtures of particles of unequal sizes (LJ σ-parameters). The influence of the relative particle masses on the dynamics should also be looked into. Moreover, the question arises if there also exists an anisotropy for other dynamical properties like the thermal conductivity or the viscosity coefficient. The latter would be particularly important in understanding the mechanical behavior of liquid interfaces.

List of symbols

A	cross-sectional area of the interface
C_{vv}	velocity autocorrelation function
D_s	self-diffusion coefficient
E_D	activation energy
$f_{ij\beta}$	β-component of force acting between particles i and j; $\beta = x, y, z$
k	Boltzmann's constant
L_x, L_y, L_z	box lengths in x, y, z-direction
N	number of particles
N_ave	number of averages in the calculation of the VACF
N_corr	number of correlated configurations in the VACF
P	pressure
r	intermolecular distance
r_cut	cut-off radius
$\dot{r}_{i\alpha}$	α-velocity of particle i; $\alpha = x, y, z$
t	time
t_corr	correlation time
Δt	time step size
T	temperature
T_c	critical temperature
$\vec{v}_i$	velocity of particle i
V	volume
w	interfacial width
x	mole fraction
z	z-coordinate
z_i	position of Gibbs' dividing surface

Greek letters

γ	interfacial tension
ϵ	Lennard–Jones potential energy parameter
ρ	density
σ	Lennard–Jones potential size parameter
ξ	factor in the Berthelot rule

Acknowledgements

This work has been supported by the European Commission Research Directorate in the context of a Marie Curie Fellowship at the LPCM at the Université Bordeaux 1 (contract no. HPMT-CT-2000-00143) and the Deutsche Forschungsgemeinschaft (DFG) (contract no. Ha1283/4-3). Computer time was provided by the Fachgebiet für Thermische Verfahrenstechnik at TU-Darmstadt. The authors want to thank especially J. Winkelmann for helpful discussions and for providing data from his DFT-calculations as well as K. Mecke for helpful correspondence. JBB also thanks PAB and his group for an instructive stay at the LPCM and for their kind hospitality.

References

[1] M. Sanyal, S. Sinha, K. Huang, B. Ocko, Phys. Rev. Lett. 66 (5) (1991) 628–631.
[2] M. Sferrezza, C. Xiao, R. Jones, D. Bucknall, J. Webster, J. Penfold, Phys. Rev. Lett. 78 (19) (1997) 3693–3696.
[3] I. Benjamin, Annu. Rev. Phys. Chem. 48 (1997) 407–451.
[4] A. Trokhymchuk, J. Alejandre, J. Chem. Phys. 111 (18) (1999) 8510–8523.
[5] M. Mecke, J. Winkelmann, J. Fischer, J. Chem. Phys. 107 (1997) 9264–9270.
[6] L.-J. Chen, J. Chem. Phys. 103 (23) (1995) 10214–10216.
[7] L. Dang, T.-M. Chang, J. Chem. Phys. 106 (19) (1997) 8149.
[8] R. Taylor, L. Dang, B. Garrett, J. Phys. Chem. 100 (1996) 11720–11725.
[9] J. Alejandre, D. Tildesley, G. Chapela, J. Chem. Phys. 102 (11) (1995) 4574–4583.
[10] A. Hariharan, J. Harris, J. Chem. Phys. 101 (5) (1994) 4156–4165.
[11] M. Nijmeijer, C. Bakker, A.F. Bruin, J. Sikkenk, J. Chem. Phys. 89 (6) (1988) 3789–3792.
[12] Z. Wang, M. Chen, Z. Guo, C. Yang, Fluid Phase Equilibria 183–184 (2001) 321–329.
[13] M. Mecke, J. Winkelmann, J. Fischer, J. Chem. Phys. 110 (2) (1999) 1188–1194.
[14] K. Schweighofer, U. Essmann, M. Berkowitz, J. Phys. Chem. B 101 (1997) 3793–3799.
[15] M. Matsumoto, Y. Takaoka, Y. Kataoka, J. Chem. Phys. 98 (2) (1993) 1464–1472.
[16] E. Diaz-Herrera, J. Alejandre, G. Ramirez-Santiago, F. Forstmann, J. Chem. Phys. 110 (16) (1999) 8084–8089.
[17] J. Stecki, S. Toxvaerd, J. Chem. Phys. 103 (10) (1995) 4352–4359.
[18] S. Toxvaerd, J. Stecki, J. Chem. Phys. 102 (18) (1995) 7163–7168.
[19] Y. Zhang, S. Feller, B. Brooks, R. Pastor, J. Chem. Phys. 103 (23) (1995) 10252–10266.
[20] P. Fernandes, M. Cordeiro, J. Gomes, J. Phys. Chem. B 103 (1999) 6290–6299.
[21] P. Fernandes, M. Cordeiro, J. Gomes, J. Mol. Struct. (Theochem) 463 (1999) 151–156.

[22] L. Dang, J. Chem. Phys. 110 (20) (1999) 10113–10122.
[23] M. Hayoun, M. Meyer, P. Turq, Chem. Phys. Lett. 147 (2–3) (1988) 203–207.
[24] M. Meyer, M. Mareschal, M. Hayoun, J. Chem. Phys. 89 (1988) 1067–1073.
[25] I. Benjamin, J. Chem. Phys. 97 (2) (1992) 1432–1445.
[26] M. Lamm, C. Hall, Fluid Phase Equilibr. 182 (2001) 37–46.
[27] M. van Leeuwen, C. Peters, J. de Swaan Arons, A. Panagiotopoulos, Fluid Phase Equilibr. 66 (1991) 57–75.
[28] A. Panagiotopoulos, ACS Symposium Series, vol. 406, 1989, pp. 39–51.
[29] J. Winkelmann, Personal communication, 2003.
[30] M. Wendland, Born–Green–Yvon results for the liquid–vapour interface of pure fluids and binary model mixtures, Fluid Phase Equilibr. 141 (1997) 25–43.
[31] M. Wendland, Liquid–liquid and liquid–vapour interfaces and wetting phenomena in the system methane–perfluoromethane calculated with the Born–Gree–Yvon equation, Fluid Phase Equilibr. 147 (1998) 105–122.
[32] H. Berendsen, J. Postma, W. van Gunsteren, A. Di Nola, J. Haak, J. Chem. Phys. 81 (1984) 3684–3690.
[33] W. Smith, T.R. Forester, DL_POLY is a package of molecular simulation routines, The Council for the Central Laboratory of the Research Councils, Daresbury Laboratory at Daresbury, Warrington, UK, 1996.
[34] S. Sides, G. Grest, M.-D. Lacasse, Phys. Rev. E 60 (6) (1999) 6708–6713.
[35] M. Mecke, Ph.D. Thesis, Martin-Luther-Universität Halle-Wittenberg, 1999.
[36] D. Beyens, M. Robert, J. Chem. Phys. 87 (5) (1987) 3056–3061.
[37] J. Huang, W. Webb, J. Chem. Phys. 50 (9) (1969) 3677–3693.
[38] J. Rowlinson, B. Widom, Molecular Theory of Capillarity, Clarendon Press, Oxford, 1982.
[39] J. van der Waals, Z. Phys. Chem. 13 (1894) 657–725. German Translation by Ostwald.
[40] R. Evans, J. Henderson, D. Hoyle, A. Parry, Z. Sabeur, Asymptotic decay of liquid structure: oscillatory liquid–vapour density profiles and the Fisher–Widom line, Mol. Phys. 80 (4) (1993) 755–775.
[41] M. Mandell, J. McTague, A. Rahman, J. Chem. Phys. 64 (9) (1976) 3699–3702.
[42] A. Rahman, M. Mandell, J. McTague, J. Chem. Phys. 64 (4) (1976) 1564–1568.
[43] H. Flyvberg, H. Petersen, J. Chem. Phys. 91 (1) (1989) 461–466.
[44] D. McQuarrie, Statistical Mechanics, Harper & Row, New York, London, 1976.
[45] H. Davis, Kinetic theory of strongly inhomogeneous fluids, Fundamentals of Inhomogeneous Fluids, Marcel Dekker, New York, 1992, pp. 551–598.
[46] P. Atkins, Physikalische Chemie, VCH Verlagsgesellschaft, Weinheim, 1996.